A Computational Study of a Spatially Continuum Mean Field Model Capturing Loss of Consciousness and the Emergence of Alpha and Gamma Rhythmic Activity in the Neocortex

Wassim M. Haddad

Abstract—In this paper, we analyze the spatio-temporal mean field model developed by Liley $\it et~al.~[1]$ in order to advance our understanding of the wide effects of pharmacological agents and anesthetics. Specifically, we use the spatio-temporal mean field model in [1] for capturing the electrical activity in the neocortex to computationally study the emergence of α -and γ -band rhythmic activity in the brain. We show that α oscillations in the solutions of the model appear globally across the neocortex, whereas γ oscillations can emerge locally as a result of a bifurcation in the dynamics of the model. We solve the dynamic equations of the model using a finite element solver package and show that our results verify the predictions made by bifurcation analysis.

I. Introduction

An important open question in neuroscience is how information is represented and transmitted in the brain by a network of neurons. Neurons may be thought of as dynamic elements that are excitable, and can generate a pulse or spike whenever the electrochemical potential across the cell membrane of the neuron exceeds a certain threshold. The Hodgkin-Huxley model [2] is the prominent model for characterizing nerve pulse propagation and relies on ion currents through ion channels (resistors) and the lipid membrane (capacitor). This model is a purely electrical model and assumes that proteins alone enable nerve cells to propagate signals due to the ability of various ion channel proteins to transport sodium and potassium ions.

A key application of dynamical systems theory to the neurosciences is to study phenomena of the central nervous system that exhibit nearly discontinuous transitions between macroscopic states. A very challenging and clinically important problem exhibiting this phenomenon is the induction of general anesthesia. In any specific patient, the transition from consciousness to unconsciousness as the concentration of anesthetic drugs increases is very sharp, resembling a thermodynamic critical phase transition.

The most likely explanation for the mechanisms of action of anesthetics lies in the network properties of the brain. It is well established that there are two general types of neurons in the central nervous system—excitatory and inhibitory—interconnected in a complex dynamical network. The action potential of a spiking neuron is propagated along the axon to synapses where chemical neurotransmitters are released that generate a postsynaptic potential on the dendrites of connected neurons. There is considerable evidence that general anesthetics alter postsynaptic potentials [3], [4]. An example of how changes in the postsynaptic potential may be applied

This work was supported in part by the National Science Foundation under Grant ECCS 1708792.

W. M. Haddad is with the School of Aerospace Engineering, Georgia Institute of Technology, Atlanta, GA 30332-0150, USA (E-mail: wm.haddad@aerospace.gatech.edu).

to the analysis of the induction of anesthesia is the view of anesthesia as a phase transition proposed by Steyn-Ross *et al* [5].

While the analysis in [5] is enlightening, a dynamical systems theory framework in terms of neuronal firing rates of a large number of interacting neurons [6] or mean field models [1], [7], [8] describing electrical potentials as continuous functions in space and time can provide a theoretical foundation for explaining the underlying neural mechanisms of action for anesthesia and unconsciousness. Furthermore, using computational analysis the synaptic drive and electrical potential dynamics, generated by excitatory and inhibitory neuron populations, can be used to predict network system changes due to changes in the dynamical system model parameters to understand how the complex neuronal network changes qualitatively with the induction of anesthesia. In that regard, firing rate models used for neocortex analysis must have sufficient generality and include parameters that can account for such key physiological changes at the single neuronal level.

Even though spatially discrete network models presented in [6] can capture an arbitrary level of cellular, synaptic, and topological detail of neuronal dynamics, they generally do not relate the resulting dynamics to clinically measurable macroscopic effects (i.e., electroencephalographic activity). To link the well-known microscopic (cellular and subcellular) targets of general anesthesia action with their macroscopic effects, we analyze the spatially continuous neural population model of [1], [7], [8]. Continuum theories describing the spatio-temporal evolution of time-averaged mean firing rates for a subpopulation of excitatory and inhibitory neurons have been shown to account for the observed electroencephalographic (EEG) spectral features of anesthetized patients [1], [7], [8]. In [9], a rigorous analysis of the well-posedness, existence, uniqueness, nonnegativity, and regularity of solutions as well as the existence, stability, and nature of attractors of this electrocortical mean field model was addressed. In this paper, we establish the relevance of this model in predicting some of the the qualitative characteristics of the anesthetic transition.

II. A CONTINUUM MEAN FIELD MODEL OF ELECTROCORTICAL ACTIVITY

As discussed in [9], the neocortex has a layered columnar structure consisting mostly of six distinctive layers. Specifically, neurons in the neocortex are organized in vertical columns, known as *cortical columns* or *macrocolumns*, which are a fraction of a millimeter wide and traverse all the layers of the neocortex from the white matter to the pial surface. As noted in the introduction, neurons are mainly classified as excitatory or inhibitory, wherein this distinction depends on whether they increase the firing rate in the coupling neurons they are communicating with, or they essentially suppress the firing rate. Inhibitory neurons are located in all the cortical column layers and contain

axons that remain within the same region where their cell body resides. Hence, they have a local range of action. Layers III, V, and VI contain pyramidal excitatory neurons that have axons that can provide long-range communication (projection) throughout the neocortex. Layer IV contains primarily star-shaped excitatory interneurons that receive sensory inputs from the thalamus. For details, see [9].

On the local level, within a cortical column, neurons are densely interconnected and involve feedforward and feedback intracortical connections. This dense and relatively homogeneous local structure of the neocortex suggests modeling a local population of functionally similar neurons by a single space-averaged neuron, which can preserve enough physiological information to capture the temporal patterns observed in spatially smoothed (averaged) EEG signals without creating excessive theoretical complexities in the mathematical analysis of the model. On the global level, in the exclusively excitatory corticocortical communication throughout the neocortex, two major patterns of connectivity are observed. Namely, a homogeneous, symmetrical, and translation invariant pattern of connections, and a heterogeneous, patchy, and asymmetrical distribution of connections. For modeling simplicity as well as due to the unavailability of detailed anatomical data, in the model that we investigate in this paper the corticocortical connectivity is assumed to be isotropic, homogeneous, symmetric, and translation invariant

To present the mathematical model, here we use the notarion that we developed in [9]. Specifically, let $\Omega=(0,\omega)\times(0,\omega)$, $\omega>0$, be an open rectangle in \mathbb{R}^2 that defines the domain of the neocortex. Each point $x=(x_1,x_2)\in\Omega$ denotes the location of a local network—possibly representing a cortical column—modeled by a space-averaged excitatory neuron and a space-averaged inhibitory neuron. Furthermore, let E denote a population of excitatory neurons and I denote a population of inhibitory neurons. For $x\in\Omega$, $t\in[0,T]$, T>0, and $X,Y\in\{\mathrm{E},\mathrm{I}\}$, we denote by $v_{\mathrm{X}}(x,t)$, measured in mV, the spatially mean soma membrane potential of a population of type X centered at x. Moreover, we denote by $i_{\mathrm{XY}}(x,t)$, measured in mV, the spatially mean postsynaptic activation of synapses of a population of type X centered at x, onto a population of type Y centered at the same point x. In addition, we denote by $w_{\mathrm{EX}}(x,t)$, measured in s⁻¹, the mean rate of corticocortical excitatory input pulses from the entire domain of the neocortex to a population of type X centered at x. Finally, we denote by $g_{\mathrm{XY}}(x,t)$, measured in s^{-1} , the mean rate of subcortical input pulses of type X to a population of type Y centered at x. Note that, by definition, $i_{\mathrm{XY}}(x,t)$, $w_{\mathrm{EX}}(x,t)$, and $g_{\mathrm{XY}}(x,t)$ are nonnegative quantities.

A continuum mean field model for electrocortical activity in the neocortex is developed in [1] and involves a system of coupled ordinary differential equations (ODEs) and partial differential equations (PDEs) given by

$$(\tau_{\rm E}\partial_t + 1)v_{\rm E}(x,t) = \frac{V_{\rm EE} - v_{\rm E}(x,t)}{|V_{\rm EE}|} i_{\rm EE}(x,t) + \frac{V_{\rm IE} - v_{\rm E}(x,t)}{|V_{\rm IE}|} i_{\rm IE}(x,t), \quad (1)$$

$$(\tau_{\rm I}\partial_t + 1)v_{\rm I}(x,t) = \frac{V_{\rm EI} - v_{\rm I}(x,t)}{|V_{\rm EI}|} i_{\rm EI}(x,t) + \frac{V_{\rm II} - v_{\rm I}(x,t)}{|V_{\rm II}|} i_{\rm II}(x,t), \quad (2)$$

$$(\partial_t + \gamma_{\rm EE})^2 i_{\rm EE}(x,t) = e \Upsilon_{\rm EE} \gamma_{\rm EE} \left[N_{\rm EE} f_{\rm E} \left(v_{\rm E}(x,t) \right) + w_{\rm EE}(x,t) + g_{\rm EE}(x,t) \right], \quad (3)$$

$$(\partial_t + \gamma_{\rm EI})^2 i_{\rm EI}(x,t) = e \Upsilon_{\rm EI} \gamma_{\rm EI} \left[N_{\rm EI} f_{\rm E} \left(v_{\rm E}(x,t) \right) + w_{\rm EI}(x,t) + g_{\rm EI}(x,t) \right], \tag{4}$$

$$(\partial_t + \gamma_{\rm IE})^2 i_{\rm IE}(x,t) = e \Upsilon_{\rm IE} \gamma_{\rm IE} \left[N_{\rm IE} f_{\rm I} \left(v_{\rm I}(x,t) \right) \right]$$

$$+g_{\rm IE}(x,t), \qquad (5)$$

$$(\partial_t + \gamma_{\rm II})^2 i_{\rm II}(x,t) = e \Upsilon_{\rm II} \gamma_{\rm II} \left[N_{\rm II} f_{\rm I} \left(v_{\rm I}(x,t) \right) + g_{\rm II}(x,t) \right], \tag{6}$$

$$\begin{split} & \left[(\partial_t + \nu \Lambda_{\rm EE})^2 - \frac{3}{2} \nu^2 \Delta \right] w_{\rm EE}(x,t) \\ & = \nu^2 \Lambda_{\rm EE}^2 M_{\rm EE} f_{\rm E} \left(v_{\rm E}(x,t) \right), \\ & \left[(\partial_t + \nu \Lambda_{\rm EI})^2 - \frac{3}{2} \nu^2 \Delta \right] w_{\rm EI}(x,t) \\ & = \nu^2 \Lambda_{\rm EI}^2 M_{\rm EI} f_{\rm E} \left(v_{\rm E}(x,t) \right), \quad (x,t) \in \Omega \times (0,T], \quad (8) \end{split}$$

with periodic boundary conditions. Here, e is the Napier constant, ∂_t denotes partial derivative with respect to t, $\Delta \triangleq \left(\frac{\partial^2}{\partial x_1^2} + \frac{\partial^2}{\partial x_2^2}\right)$ is the Laplace operator, and $f_{\rm X}(\cdot)$ is the mean firing rate function of a population of type X and, for ${\rm X} \in \{{\rm E},{\rm I}\}$, is given by

$$f_{\rm X}(v_{\rm X}(x,t)) \triangleq \frac{{\rm F}_{\rm X}}{1 + \exp\left(-\sqrt{2}\frac{v_{\rm X}(x,t) - \mu_{\rm X}}{\sigma_{\rm X}}\right)}.$$
 (9)

The definition of the biophysical parameters of the model and the range of values they can take are given in Table I. For the range of values given in Table I, $|V_{\rm EE}|=V_{\rm EE},$ $|V_{\rm EI}|=V_{\rm EI},$ $|V_{\rm IE}|=-V_{\rm IE}$, and $|V_{\rm II}|=-V_{\rm II}.$ As discussed in [9], (1) and (2) model the dynamics of the

As discussed in [9], (1) and (2) model the dynamics of the resistive-capacitive membrane of the space-averaged neurons located at x. In the absence of postsynaptic i-inputs, the mean membrane potential decays exponentially to the resting potential. The fractions appearing in the equations weigh the postsynaptic inputs to incorporate the effect of transmembrane diffusive ion flows into the model. Specifically, the depolarizing effect of excitatory inputs on the membrane is linearly decreased by the weights as the membrane potential rises to the Nernst (reversal) potential. When the membrane potential exceeds the Nernst potential, the effect is reversed and further excitation tends to hyperpolarize the membrane. The weights associated with the inhibitory postsynaptic inputs have opposite signs at the resting potential, and hence, they have an opposite reversal effect.

The critically damped second-order dynamics in (3)–(6) generates a synaptic α -function—analogous to classical dendritic cable theory—in response to an impulse. These second order dynamical systems are driven by three different sources of presynaptic spikes, namely, the inputs $N_{\rm XY} f_{\rm X}(v_{\rm X})$ from local neuronal populations, the excitatory inputs $w_{\rm EX}$ form corticocortical fibers, and the inputs $g_{\rm XY}$ from subcortical regions. Hence, (3)–(6) generate the postsynaptic responses modulating the polarization of the cell membranes through (1) and (2).

Unlike the conduction through short-range intracortical fibers, the conduction through long-range corticocortical fibers cannot be assumed to be instantaneous. Equations (7) and (8) form a system of telegraph equations that effectively models the propagation of the excitatory axonal pulses through corticocortical fibers. These equations are derived by assuming that the strength of corticocortical connections onto a local population decays exponentially with distance, with the characteristic scale $\Lambda_{\rm EX}$ [1]. In addition, it is assumed that the spatial distribution of connections is isotropic and homogeneous over the neocortex. The key variable in the model given by (1)–(8) is the mean membrane potential

TABLE I: Definition and range of values for the biophysical parameters of the mean field model (1)–(8). All electric potentials are given with respect to the mean resting soma membrane potential $v_{\text{rest}} = -70 \text{ mV}$ [8].

| Parameter | Definition | Range | Unit |
|---|---|---------------|--------------------|
| $	au_{ m E}$ | Passive excitatory membrane decay time constant | [0.005, 0.15] | S |
| $	au_{ m I}$ | Passive inhibitory membrane decay time constant | [0.005, 0.15] | S |
| $V_{\rm EE},V_{\rm EI}$ | Mean excitatory Nernst potentials | [50, 80] | mV |
| V_{IE}, V_{II} | Mean inhibitory Nernst potentials | [-20, -5] | mV |
| $\gamma_{\rm EE},\gamma_{\rm EI}$ | Excitatory postsynaptic potential rate constants | [100, 1000] | s^{-1} |
| $\gamma_{ m IE},\gamma_{ m II}$ | Inhibitory postsynaptic potential rate constants | [10, 500] | s^{-1} |
| $\Upsilon_{ m EE},\Upsilon_{ m EI}$ | Amplitude of excitatory postsynaptic potentials | [0.1, 2.0] | mV |
| $\Upsilon_{\mathrm{IE}},\Upsilon_{\mathrm{II}}$ | Amplitude of inhibitory postsynaptic potentials | [0.1, 2.0] | mV |
| $N_{\rm EE},N_{\rm EI}$ | Number of intracortical excitatory connections | [2000, 5000] | _ |
| N_{IE}, N_{II} | Number of intracortical inhibitory connections | [100, 1000] | _ |
| ν | Corticocortical conduction velocity | [100, 1000] | cm/s |
| $\Lambda_{ m EE},\Lambda_{ m EI}$ | Decay scale of corticocortical excitatory connectivities | [0.1, 1.0] | cm^{-1} |
| M_{EE}, M_{EI} | Number of corticocortical excitatory connections | [2000, 5000] | _ |
| $F_{\rm E}$ | Maximum mean excitatory firing rate | [50, 500] | s^{-1} |
| F_{I} | Maximum mean inhibitory firing rate | [50, 500] | s^{-1} |
| $\mu_{ m E}$ | Excitatory firing threshold potential | [15, 30] | mV |
| $\mu_{ m I}$ | Inhibitory firing threshold potential | [15, 30] | mV |
| $\sigma_{ m E}$ | Standard deviation of excitatory firing threshold potential | [2, 7] | mV |
| $\sigma_{ m I}$ | Standard deviation of inhibitory firing threshold potential | [2, 7] | mV |

of excitatory populations $v_{\rm E}(x,t)$ and is assumed to be linearly proportional to EEG recordings from the scalp [1]. For further details of the model see [1].

This model has several advantages over the model proposed in [6] in developing a macroscopic analysis of the cortical activity in the brain [9]. Specifically, the neurophysiological basis of this model has been fairly well established [1] and the definitions as well as the ranges of the values of the parameters appearing in the model are given in [1]. Furthermore, the model is derived using the well-established columnar topology of the neocortex [1], [10]. In addition, the mean membrane potential directly appears in the model, which facilitates prediction and understanding of the dynamics associated with the EEG signals available from experimental data on the brain [11]. Finally, the model is a spatio-temporal model, and hence, can be used to study dynamic EEG pattern formations in the cortex.

Preliminary numerical investigations of the proposed model have revealed that it can predict the key macroscopic electrocortical activities of the cortex. Recent patient data [12] reveal that the anesthetic propofol gives rise to a frontal α -rhythm in the EEG at drug levels sufficient to induce loss of consciousness, which shows that the proposed continuum model can capture the electro-rythmogenesis in the EEG of an anesthetized patient. The model shows that a synchronized γ activity emerges in the excitatory membrane potential when the amplitude of the inhibitory post synaptic potential is gradually decreased [7]; also an experimentally verified effect [12]. Furthermore, this model has been used to model the anesthetic cascade in the cortex [5], as well as investigate the effects of anesthesia on EEG signals [8].

Moreover, it is the only model that has numerically demonstrated the *drug biphasic response* [5], [13], wherein the administration of increasing anesthetic dose can lead to a paradoxical state of excitement prior to decreases in the level of consciousness. Specifically, the model predicts the phase

transition and burst suppression in cortical neurons during general anesthesia [5]. Furthermore, the model predicts the effect of anesthetic drugs on the EEG [14] as well as the generation of epileptic seizures [15]. In [16], the authors have used open-source computational tools to analyze the underlying PDEs of the model and solve for the model equilibria and time-periodic solutions. A rigorous analysis of the existence, uniqueness, nonnegativity, and regularity of solutions as well as the existence, stability, and nature of absorbing sets and attractors of the model is presented in [9].

In the remainder of the paper, we use appropriate finite element-based software to analyze the spatio-temporal behavior of this model. The attractor(s) of the model can be characterized to identify periodic, pseudo-periodic, chaotic, and stationary solutions. Establishing the existence or non-existence of periodic solutions can clarify all the underlying mechanisms of the α - and γ -band rhythms observed in the electrocortical activity and whether they are stochastic or deterministic oscillations.

The rhythmic patterns of variations in the electroencephalographic recordings from the scalp (EEG), or the electrocorticographic recordings from the surface of the neocortex (ECoG) demonstrate a salient feature of mesoscopic electrical activity in the neocortex. These *brain rhythms* correlate with the numerous states of healthy operation of the brain, and their possible distortion or disruption can be a signature of a certain disease or a transition from consciousness to unconsciousness. However, the physiological mechanism of generating the brain rhythms is not well-understood.

The rhythmicity in the electrocortical activity is a dynamic phenomenon that can occur, possibly heterogeneously, in a wide area of the neocortex. Hence, a mathematical model of the brain rhythms should capture both spatial and temporal dynamics of the neocortex. Such mesoscopic spatio-temporal models can effectively be developed by constructing approx-

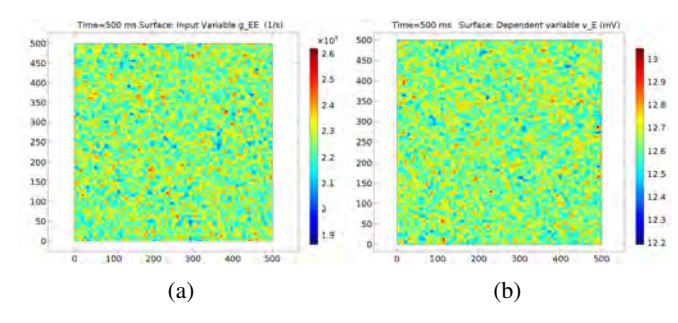


Fig. 1: Comparison of the random input $g_{\rm EE}$ and the membrane potential $v_{\rm E}$ at the resting state. (a) The random input $g_{\rm EE}$ at t=500 ms. (b) The membrane potential $v_{\rm E}$ at t=500 ms.

imate models for interconnected populations of neurons in the neocortex using mean field theory. Here, we use the spatio-temporal mean field model to study the α - and γ -band rhythmic activity in the cortex. As noted above, this model has been widely used in the literature to study brain rhythms, general anesthesia, and epileptic seizures [5], [7], [14], [15].

In the remainder of the paper, we rederive some of the computational results in [7] and analyze them in more detail. These results show that the model can generate α -band oscillations (8 - 13 Hz) at the resting state, and γ -band oscillations (30 - 80 Hz) as a result of a subcritical Hopf bifurcation in its dynamics. We use MatCont [17] to perform the numerical bifurcation analysis, and we solve the equations of the model using COMSOL Multiphysics $^{\circledR}$.

III. COMPUTATIONAL FRAMEWORK

For the computational analysis of the next sections, we consider (1)–(8) with a rectangular domain $\Omega=(0,500)\times(0,500)$ [mm²] and with the set of parameter values given in Table II. The space-homogeneous equilibrium of the model can be calculated as

$$(v_{\rm E}, v_{\rm I})_{\rm e} = (12.6326, 13.319),$$
 (10)
 $(i_{\rm EE}, i_{\rm EI}, i_{\rm IE}, i_{\rm II})_{\rm e} = (49.0506, 28.3164, 11.4371, 4.1846),$

(11)

$$(w_{\rm EE}, w_{\rm EI})_{\rm e} = (2245.7, 2057.1),$$
 (12)

where the numbers are regarded as constant functions over the domain Ω . We set the time horizon of the numerical computations at T=500 ms, and use COMSOL Multiphysics $^{\circledR}$ to solve (1)–(8) with periodic boundary conditions and with the initial values and input variables as specified in the following sections.

To draw quantitative observations on the transitions of the computed solutions in time, we extract samples from the solution data at different locations over Ω . To approximately simulate the averaging effect of an EEG probe, we extract solution data over squares of size 10×10 [mm²], which we refer to as probes. We then consider the measurement of a probe as the average value of the solution over the square domain of the probe, which gives a scalar-valued signal over [0,T].

IV. ALPHA RHYTHMS IN THE RESTING STATE

To observe α -band oscillations, we consider the resting state with the nominal parameter values as given in Table II. We drive the model by an input $g_{\rm EE}$, which varies randomly in space and time about the mean value $\bar{g}_{\rm EE}$ given in Table II. A snapshot of $g_{\rm EE}$ that depicts a sample of its pattern

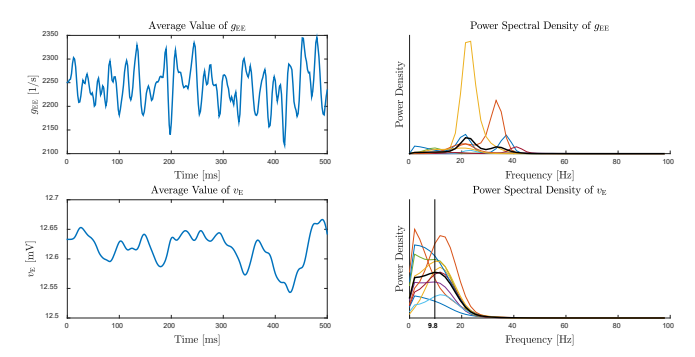


Fig. 2: Time and frequency analysis of the α oscillations. Left: Measurements of the random input $g_{\rm EE}$ and the membrane potential $v_{\rm E}$ at a randomly chosen probe location. Right: Power spectral density of the measurements of ten probes located randomly over the domain of the neocortex Ω . The solid black curve is the average of the power densities of the ten measurements. The zero-frequency components (mean value) of all signals are removed.

of variations over Ω is shown in Figure 1a. The other inputs $g_{\rm EI}$, $g_{\rm IE}$, and $g_{\rm II}$ take the constant values $\bar{g}_{\rm EI}$, $\bar{g}_{\rm IE}$, and $\bar{g}_{\rm IE}$ given in Table II, respectively. Finally, we set the initial values $(v_{\rm E}, v_{\rm I}, i_{\rm EE}, i_{\rm EI}, i_{\rm IE}, i_{\rm II}, w_{\rm EE}, w_{\rm EI})\big|_{t=0}$ equal to their equilibrium values given by (10)–(12), and the initial values $d_t(i_{\rm EE}, i_{\rm EI}, i_{\rm IE}, i_{\rm II}, w_{\rm EE}, w_{\rm EI})\big|_{t=0}$ equal to zero.

Figure 1b shows the result of the numerical computations for $v_{\rm E}$ at the final time step t=500 ms. As compared with Figure 1a, we observe that $v_{\rm E}$ does not develop any specific spatial pattern of activity and essentially shows a similar pattern of random variations as observed in the input $g_{\rm EE}$. However, as shown in Figure 2, oscillations in $v_{\rm E}$ are primarily in the α -band, whereas the random input is oscillating at distinctively higher frequencies.

V. EMERGENCE OF GAMMA RHYTHMS

In this section, we show that oscillations in the γ -band can emerge in the solutions of the model as a result of a subcritical Hopf bifurcation. In order to effectively use the available numerical bifurcation analysis tools, we consider a space-homogeneous version of the model (1)–(8). This corresponds to the solutions of the model with space-homogeneous initial values and input variables. As a result, (1)–(8) is transformed to a fourteenth-order system of ODEs by setting $-\frac{3}{2}\nu^2\Delta=0$.

Then, as in [7], we consider the bifurcation analysis of the resulting ODE system with respect to variations in the number of inhibitory to inhibitory intracortical connections $N_{\rm II}.$ The excitation of interneurons in layer IV by thalamic afferents is proposed in [7] as a mechanism for presynaptic facilitation of the inhibitory to inhibitory connections, which can be modeled by increasing $N_{\rm II}.$ Specifically, we replace $N_{\rm II}$ by $\eta N_{\rm II},$ where $\eta>0$ adjusts the percentage of the deviation of $N_{\rm II}$ from its nominal value given in table II.

We use MatCont to rederive the bifurcation analysis given in [7]. The results are shown in Figure 3. As we see in Figure 3, increasing $N_{\rm II}$ from its nominal value by a factor of $\eta=1.0676$ results in a subcritical Hopf bifurcation, and the dynamics of the model undergoes a phase transition from damped oscillations about the stable equilibrium to sustained oscillations on a stable limit cycle. These results, which are derived based on the space-homogeneous ODE version of the model, predict the emergence of oscillatory patterns of activity in the original model (1)–(8) as a result of an increase in $N_{\rm II}$. In the following, we verify this prediction

TABLE II: The set of biophysically plausible parameter values used for the computational analysis of the model (1)–(8) [8, Table V, col. 11]. The parameters \bar{g}_{EE} , \bar{g}_{EI} , \bar{g}_{IE} , and \bar{g}_{II} are, respectively, the mean values of the physiologically shaped random inputs g_{EE} , g_{EI} , g_{IE} , and g_{II} used in [8].

| Parameter | $	au_{ m E}$ | $	au_{ m I}$ | V_{EE} | $ m V_{EI}$ | $ m V_{IE}$ | V_{II} | $\gamma_{ m EE}$ | $\gamma_{ m EI}$ |
|-----------|---------------------------|--------------------------|--------------------|--------------------------------------|--------------------------|--------------------------|--------------------|--------------------|
| Value | $32.209_{\times 10^{-3}}$ | $92.26_{\times 10^{-3}}$ | 79.551 | 77.097 | -8.404 | -9.413 | 122.68 | 982.51 |
| Parameter | $\gamma_{ m IE}$ | $\gamma_{ m II}$ | $\Upsilon_{ m EE}$ | $\Upsilon_{ m EI}$ | Υ_{IE} | Υ_{II} | N_{EE} | $N_{\rm EI}$ |
| Value | 293.1 | 111.4 | 0.29835 | 1.1465 | 1.2615 | 0.20143 | 4202.4 | 3602.9 |
| Parameter | $ m N_{IE}$ | $ m N_{II}$ | ν | $\Lambda_{\rm EE}, \Lambda_{\rm EI}$ | ${ m M_{EE}}$ | $ m M_{EI}$ | $\mathrm{F_{E}}$ | $\mathrm{F_{I}}$ |
| Value | 443.71 | 386.43 | 116.12 | 0.6089 | 3228 | 2956.9 | 66.433 | 393.29 |
| Parameter | $\mu_{ m E}$ | $\mu_{ m I}$ | $\sigma_{ m E}$ | $\sigma_{ m I}$ | $ar{g}_{	ext{EE}}$ | $ar{g}_{	ext{EI}}$ | $ar{g}_{	ext{IE}}$ | $ar{g}_{	ext{II}}$ |
| Value | 27.771 | 24.175 | 4.7068 | 2.9644 | 2250.6 | 4363.4 | 0 | 0 |

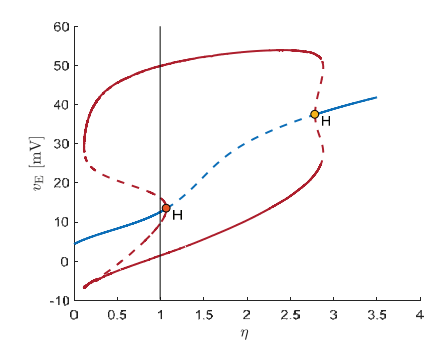


Fig. 3: The bifurcation diagram associated with the space-homogenous ODE version of (1)–(8). The bifurcation parameter η indicates the percentage of the deviation of $N_{\rm II}$ from its nominal value. The curve of equilibria is shown in blue, and the curves of the maximum and minimum values of the limit cycles are shown in red. Solid lines denote stable equilibria and limit cycles, and dashed lines denote unstable equilibria and limit cycles. The two Hopf bifurcation points are marked by H.

by computing the solutions of (1)–(8), and show that the frequency of these oscillations is in the γ -band.

For the numerical computations, we set N_{II} equal to $\eta = 1.07$ times the nominal value given in Table II. We set $(g_{\rm EE},g_{\rm EI},g_{\rm IE},g_{\rm II})=(\bar{g}_{\rm EE},\bar{g}_{\rm EI},\bar{g}_{\rm IE},\bar{g}_{\rm IE})$ and perform the computations by setting the initial value of $v_{\rm E}$ equal to the function shown in Figure 4a, while setting the other initial values equal to their equilibrium values given by (10)–(12). Figure 5 shows snapshots of $v_{\rm E}$ at different time instances. We observe that specific patterns of oscillations emerge spontaneously and propagate throughout the neocortex. To measure the power spectral density of these oscillations, we set eight measurement probes F1–F8 at the focal points of these spatial patterns, as shown in Figure 4b. Moreover, we set eight measurement probes B1-B8 at other background locations to observe the oscillations in regions of the neocortex that do not develop any salient patterns of activity during the time horizon of the computation. The measurements of the probes are shown in Figures 6 and 7, and their power spectral densities are shown in Figure 8. We observe that the power spectrum of the spatial patterns of oscillations that emerge locally in the neocortex lies essentially in the γ -band, whereas oscillations at other areas remain in the α band. This observation shows that γ oscillation can occur locally in the cortex, possibly in regions that are engaged with certain cognitive tasks.

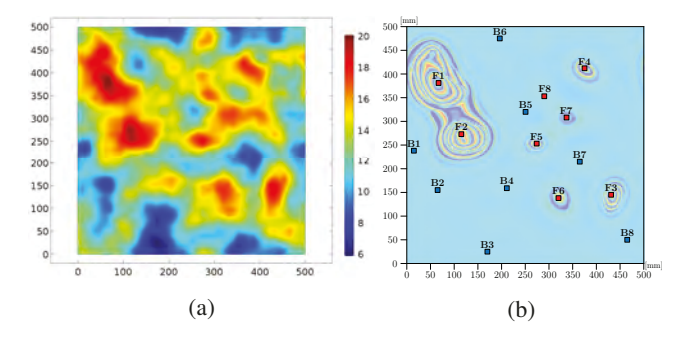


Fig. 4: (a) The initial value of $v_{\rm E}$ in mV. (b) The locations of the measurement probes used to extract signals for the time and frequency analysis of the γ -rhythms.

VI. CONCLUSION

In this paper, we used a spatio-temporal mean field model of the electroencephalographic activity in the neocortex to study the rhythmic activity in the brain. We showed, through bifurcation analysis and numerical computations, that this model can generate α - and γ -rhythms. The γ oscillations in the solutions of the model emerged as a result of an increase in the number of inhibitory to inhibitory intracortical connections. Furthermore, we showed that during the time the γ oscillations emerge locally in different regions of the neocortex, oscillations at other regions can still remain in the α -band.

Acknowledgment. The author thanks Farshad Shirani for performing the numerical simulations in the paper.

REFERENCES

- [1] D. T. J. Liley, P. J. Cadusch, and M. P. Dafilis, "A spatially continuous mean field theory of electrocortical dynamics," *Network: Comput. Neural Syst.*, vol. 13, pp. 67–113, 2002.
- [2] A. L. Hodgkin and A. F. Huxley, "A quantitative description of membrane current and application to conduction and excitation in nerve," *J. Physiol.*, vol. 117, pp. 500–544, 1952.
- [3] A. Kiyamura, W. Marszalec, J. Z. Yeh, and T. Narahishi, "Effects of halothane and propofol on excitatory and inhibitory synaptic transmission in rat cortical neurons," *J. Pharmacol.*, vol. 304, pp. 162– 171, 2002.
- [4] A. Hutt and A. Longtin, "Effects of the anesthetic agent propofol on neural populations," Cogn. Neurodyn., vol. 4, pp. 37–59, 2009.

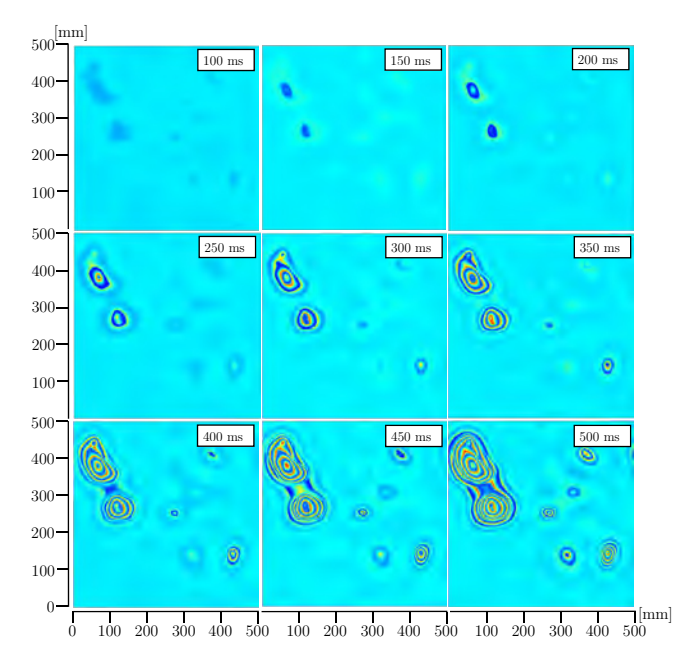


Fig. 5: Emergence of γ -band rhythmic activity. Snapshots are taken from $v_{\rm E}$ at every 50 ms.

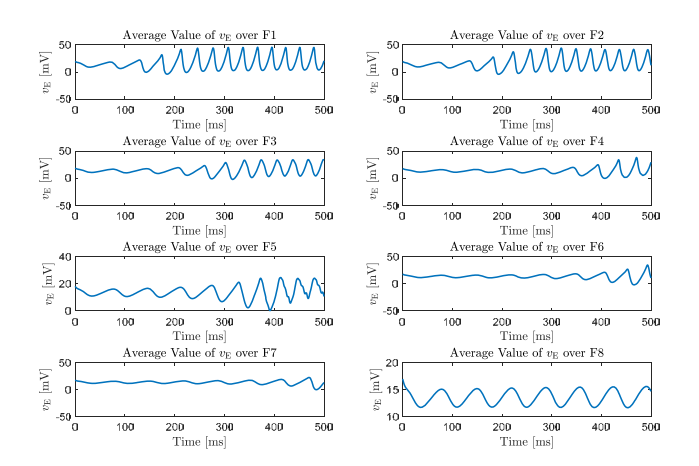


Fig. 6: Measurements of F1-F8 probes at the locations shown in Figure 4b.

- [5] M. L. Steyn-Ross, D. A. Steyn-Ross, and J. W. Sleigh, "Modelling general anaesthesia as a first-order phase transition in the cortex," *Progress in Biophysics and Molecular Biology*, vol. 85, no. 2–3, pp. 369–385, 2004.
- [6] S. P. Hou, W. M. Haddad, N. Meskin, and J. M. Bailey, "A mechanistic neural mean field theory of how anesthesia suppresses consciousness: Synaptic drive dynamics, system stability, attractors, partial synchronization, and the anesthetic cascade," *J. Math. Neuroscience*, vol. 2015, pp. 1–50, 2015.
- [7] I. Bojak and D. T. J. Liley, "Self-organized 40 Hz synchronization in a physiological theory of EEG," *Neurocomputing*, vol. 70, pp. 2085– 2090, 2007.
- [8] —, "Modeling the effects of anesthesia on the electroencephalogram," *Phys. Rev. E*, 71:041902, 2005.
- [9] F. Shirani, W. M. Haddad, and R. de la Llave, "On the global dynamics of an electroencephalographic mean field model of the neocortex," *SIAM Journal on Applied Dynamical Systems*, vol. 16, no. 4, pp. 1969– 2029, 2017.
- [10] E. R. Kandel, J. H. Schwartz, T. M. Jessell, S. A. Siegelbaum, and A. J. Hudspeth, *Principles of Neural Science*. New York, NY, USA: McGraw-Hil, 2013.

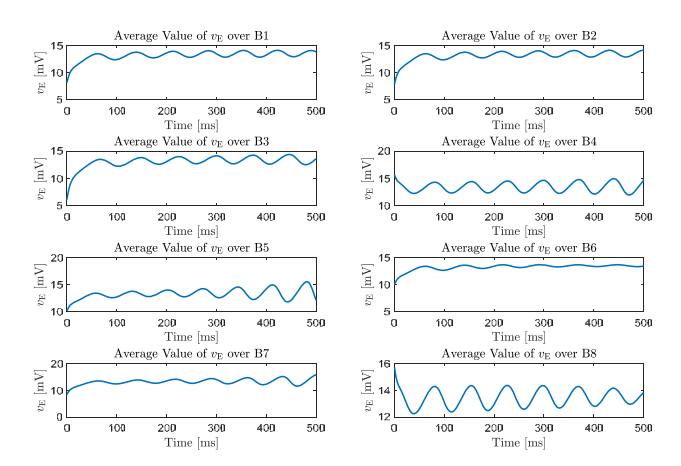


Fig. 7: Measurements of B1-B8 probes at the locations shown in Figure 4b.

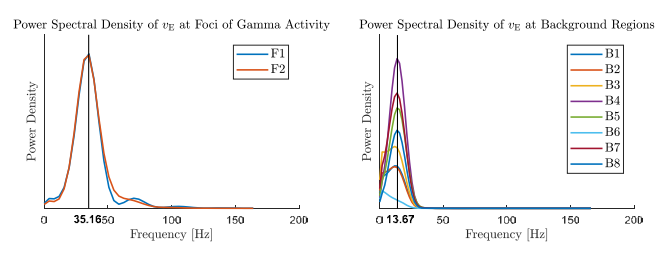


Fig. 8: Power spectral density of the measurements of F1, F2, and B1–B8 probes shown in Figures 6 and 7. The zero-frequency components (mean value) of all signals are removed. Power densities are calculated based on the last 256 ms measurements of F1 and F2 probes and the last 400 ms measurements of the B1–B8 probes to remove the effect of the initial period of transitions on the spectrum.

- [11] G. A. Mashour, "Consciousness and the 21st century operating room," Anesthesiology, vol. 119, no. 5, pp. 1003–1005, 2013.
- [12] S. Ching, A. Cimenser, P. L. Purdon, E. N. Brown, and N. J. Kopell, "Thalamocortical model for a propofol-induced α-rhythm associated with loss of consciousness," *Proc. Nat. Acad. Sci.*, vol. 107, no. 52, pp. 22 665–22 670, 2010.
- [13] K. Kuizenga, J. Wierda, and C. Kalkman, "Biphasic EEG changes in relation to loss of consciousness during induction with thiopental, propofol, etomidate, midazolam or sevoflurane," *Br. J. Anaesth.*, vol. 86, no. 3, pp. 354–360, 2001.
- [14] I. Bojak, H. C. Day, and D. T. J. Liley, "Ketamine, propofol and the EEG: A neural field analysis of HCN1-mediated interactions," *Frontiers in Computational Neuroscience*, vol. 7, no. 22, 2013.
- [15] M. A. Kramer, H. E. Kirsch, and A. J. Szeri, "Pathological pattern formation and cortical propagation of epileptic seizures," *Journal of the Royal Society Interface*, vol. 2, pp. 113–127, 2005.
- [16] K. R. Green and L. van Veen, "Open-source tools for dynamical analysis of Liley's mean-field cortex model," *Journal of Computational Science*, vol. 5, no. 3, pp. 507–516, 2014.
- [17] A. Dhooge, W. Govaerts, Y. A. Kuznetsov, H. G. E. Meijer, and B. Sautois, "New features of the software matcont for bifurcation analysis of dynamical systems," *Math. Comput. Model. Dyn. Syst.*, vol. 14, no. 2, pp. 147–175, 2008. [Online]. Available: https://doi.org/10.1080/13873950701742754